INTERFACE

rsif.royalsocietypublishing.org

Research

**Cite this article:** Blanke A, Schmitz H, Patera A, Dutel H, Fagan MJ. 2017 Form–function relationships in dragonfly mandibles under an evolutionary perspective. *J. R. Soc. Interface* **14**: 20161038.
http://dx.doi.org/10.1098/rsif.2016.1038

Received: 21 December 2016
Accepted: 2 March 2017

**Subject Category:**
Life Sciences–Engineering interface

**Subject Areas:**
biomechanics, evolution

**Keywords:**
insect, finite element analysis, geometric morphometrics, functional morphology, phylogeny

**Author for correspondence:**
Alexander Blanke
e-mail: a.blanke@hull.ac.uk

Electronic supplementary material is available online at https://dx.doi.org/10.6084/m9.figshare.c.3715243.

THE ROYAL SOCIETY PUBLISHING

# Form–function relationships in dragonfly mandibles under an evolutionary perspective

Alexander Blanke[1], Helmut Schmitz[2], Alessandra Patera[3,4], Hugo Dutel[1] and Michael J. Fagan[1]

[1]Medical and Biological Engineering Research Group, School of Engineering, University of Hull, Hull HU6 7RX, UK
[2]Institute for Zoology, University of Bonn, Poppelsdorfer Schloss, 53115 Bonn, Germany
[3]Swiss Light Source, Paul Scherrer Institut, Villigen 5232, Switzerland
[4]Centre d'Imagerie BioMedicale, Ecole Polytechnique Federale de Lausanne, 1015 Lausanne, Switzerland

AB, 0000-0003-4385-6039

Functional requirements may constrain phenotypic diversification or foster it. For insect mouthparts, the quantification of the relationship between shape and function in an evolutionary framework remained largely unexplored. Here, the question of a functional influence on phenotypic diversification for dragonfly mandibles is assessed with a large-scale biomechanical analysis covering nearly all anisopteran families, using finite element analysis in combination with geometric morphometrics. A constraining effect of phylogeny could be found for shape, the mandibular mechanical advantage (MA), and certain mechanical joint parameters, while stresses and strains, the majority of joint parameters and size are influenced by shared ancestry. Furthermore, joint mechanics are correlated with neither strain nor mandibular MA and size effects have virtually play no role for shape or mechanical variation. The presence of mandibular strengthening ridges shows no phylogenetic signal except for one ridge peculiar to Libelluloidea, and ridge presence is also not correlated with each other. The results suggest that functional traits are more variable at this taxonomic level and that they are not influenced by shared ancestry. At the same time, the results contradict the widespread idea that mandibular morphology mainly reflects functional demands at least at this taxonomic level. The varying functional factors rather lead to the same mandibular performance as expressed by the MA, which suggests a many-to-one mapping of the investigated parameters onto the same narrow mandibular performance space.

## 1. Introduction

Insects show a remarkable variety of mouthparts, but the factors leading to this variety are poorly understood. It is unclear at which levels mouthpart form is mainly regulated by functional requirements such as food spectrum or weight optimization, and when phylogeny or development play a major role [1–4]. Surprisingly few studies have assessed the mechanical performance of insect mandibles. So far, insect mandible bite performance has been shown to be influenced by the origin and attachment sites of the mandible muscles [5–8], muscle mass, muscle physiology and structure, as well as innervations [8–12]. Distantly related lineages such as beetles and grasshoppers show larger differences in mandible shape [13,14], which is presumably related to different food types [15–17].

Owing to the high diversity in the shape of mouthparts across insects, the influences of function and phylogeny are difficult to separate from each other, and from other factors such as the ecological niche or development. In this context, dragonflies represent a useful model system, because their lifestyle and mouthpart morphology are comparably uniform. All dragonflies are aerial hunters that prey on other winged insects such as flies, mosquitoes or even other dragonflies, which they often consume on the wing, and they show the same larval development with several stages of aquatic larvae before moulting (with a drastic morphological

reorganization) to the adult [18]. Mandible gross morphology is also the same among all adult dragonflies with a row of sharp teeth-like structures (incisivi) in the apical position and another row of subapical incisivi in the mesal area and a similar shape overall [19,20]. Thus, their ecomorphology with regards to food uptake and potential developmental constraints is largely similar. Given these similarities, it should be possible to study the influence of small morphological variations on function with the background of a phylogenetic framework. Here, we use a group of dragonfly species which show the same muscular arrangement, the same joint type and the same gross mandibular form to investigate the interplay of shape and biomechanics and the influence of phylogeny on these factors. In particular, we study whether shape, biomechanics or size show a phylogenetic signal and whether shape, biomechanics and size correlate with each other.

## 2. Material and methods

We used the damselfly *Calopteryx virgo* and a range of dragonfly species (Odonata: Anisoptera) covering all currently recognized families except Chlorogomphidae and Synthemistidae (table 1) for our analyses. The resulting dataset consisted of 21 mandible models. All samples are housed in the alcohol collection of the Zoological Research Museum Alexander Koenig (ZFMK). For the sake of brevity, species are named only with their genus name in the following. The description of morphological structures follows the terminology of Beutel *et al*. [21]. New terms for mandible structures not covered so far in the literature are defined at the appropriate points in the text when they are first used.

### 2.1. Bite force measurements

In order to understand how bite force influences strain levels, we measured the bite force of five out of the 21 studied species (*Sympetrum*, *Cordulegaster*, *Onychogomphus*, *Aeshna* and *Anax*), covering a wide range of body size and taxonomy, that were available locally (collection permit 67.1-2.03.20-33/13-M (ZFMK)). Bite force measurements were performed using a bespoke set-up described in other studies [22,23]. Briefly, it consisted of a custom-built specimen fixation device and an adjustable piezoelectric mini-force sensor (SKB pinforce sensor Z18152X2A3sp and Z18152X2A7sp; Kistler, Winterthur, Switzerland). Bite series were filtered (Butterworth, low pass, fourth order, 50 Hz cut-off, recursive), and single bites were identified when the force–time curve showed a continuous increase of at least 0.02 N, an unambiguously identifiable absolute maximum, absence of local minima between biting onset and peak force, and absence of movement artefacts owing to movement of the insect. Please refer to David *et al*. [22,23] for further details.

### 2.2. Mechanical testing via nano-indentation

We used the same set of freshly collected dragonflies for measuring the material parameters of the mandibles. Mandibles were excised and embedded in Epoxy Resin L (R&G Faserverbundwerkstoffe, Germany). Semi-thin cross sections were cut from the embedded samples, using a microtome equipped with a 6 mm diamond knife (Diatome, Switzerland), in 4 µm slices until a suitable cross-sectional profile was identified, at which point the surface was polished by cutting a few ultrathin sections at 0.5 µm.

An area function covering all contact depths obtained in the measurements was established by indenting a polymethyl methacrylate test specimen of known hardness and modulus. To obtain data from cuticle that is fully saturated with water, a drop of distilled water was put on the faces of the resin blocks for at least 20 min before the test; this was sufficient to saturate the material and stabilize the material properties [24]. After this, an appropriate position for indentation was located and another drop of distilled water was placed between the surface and tip to ensure wet cuticle properties. After another 5–10 min, the water was removed again and measurements ($N = 6$–15 per sample at locations at least 4 µm apart) were taken in rapid succession, typically every 15 s. This measurement process followed a protocol optimized in earlier studies [24,25] and ensured that wet cuticle properties were measured. Contact depths ranged from 130 to 1500 nm, with a maximum load during indentation of 1500 µN and loading and unloading rates of 20 µN $s^{-1}$, and a 2 s holding time at peak load to compensate for material creep. Hardness (H) and reduced Young's modulus (E) were both determined from the unloading portions of the load–displacement curves following established procedures [26].

**Table 1.** Taxon sampling used and overview of head sizes and mandible ridge presence. AAR, anterior acetabular ridge; PCR, posterior condylar ridge; MR, median ridge; LR, lateral ridge.

| family | species | head width (mm) | AAR | PCR | MR | LR |
|---|---|---|---|---|---|---|
| Zygoptera | *C. splendens* | 6.12 | 0 | 0 | 0 | 0 |
| Epiophlebiidae | *E. superstes* | 7.72 | 0 | 0 | 0 | 0 |
| Gomphidae | *O. forcipatus* | 9.70 | 1 | 1 | 0 | 0 |
| Gomphidae | *H. brevistylus* | 10.55 | 1 | 0 | 0 | 1 |
| Gomphidae | *Z. batesi* | 9.59 | 1 | 0 | 0 | 1 |
| Petaluridae | *P. raptor* | 11.61 | 1 | 0 | 0 | 1 |
| Petaluridae | *T. thoreyi* | 10.90 | 0 | 0 | 0 | 1 |
| Aeshnidae | *A. imperator* | 9.88 | 1 | 0 | 0 | 0 |
| Aeshnidae | *A. mixta* | 8.38 | 1 | 0 | 0 | 1 |
| Aeshnidae | *A. anisoptera* | 10.69 | 1 | 0 | 0 | 1 |
| Aeshnidae | *A. isoceles* | 9.61 | 0 | 1 | 0 | 0 |
| Aeshnidae | *O. pryeri* | 8.53 | 0 | 0 | 0 | 0 |
| Austropetaliidae | *P. apicalis* | 9.74 | 0 | 0 | 0 | 0 |
| Cordulegastridae | *A. sieboldii* | 12.57 | 1 | 1 | 0 | 0 |
| Cordulegastridae | *C. bidentata* | 8.69 | 1 | 1 | 0 | 0 |
| Neopetaliidae | *N. punctata* | 8.97 | 0 | 1 | 0 | 0 |
| Libelluloidea | *M. taeniolata* | 10.00 | 1 | 0 | 1 | 1 |
| Libelluloidea | *E. elegans* | 10.78 | 0 | 0 | 1 | 1 |
| Libelluloidea | *C. aenea* | 8.12 | 1 | 0 | 1 | 1 |
| Libelluloidea | *S. vulgatum* | 5.22 | 0 | 0 | 1 | 0 |
| Libelluloidea | *L. depressa* | 8.21 | 0 | 0 | 1 | 0 |

### 2.3. Three-dimensional model generation

To obtain models of the mandibles suitable for finite element analysis (FEA), we performed synchrotron radiation micro-computed tomography (SR-µCT). For preparation, collected odonates were either freshly placed into Bouin solution [27] or taken from the alcohol collection at ZFMK. Samples were washed in 70% EthOH, critical point dried (model E4850; BioRad), and mounted on specimen holders. SR-µCT was carried out at the Deutsches Elektronen Synchrotron (beamlines DORIS III/BW2 and PETRA III/IBL P05; DESY, Hamburg, Germany) or at the Swiss Light Source of the Paul-Scherrer Institut (PSI; Villigen, Switzerland; beamline TOMCAT) using established procedures [28–30]. Subsequent segmentation of the reconstructed image stacks was accomplished with ITK-SNAP [31]. STL files were then imported into AVIZO (v. 9.0.1; FEI, USA) for generation of the tetrahedral meshes which were then exported in UNV format for import into the finite element (FE) solver. We plotted the cuticle thickness on the three-dimensional models of the mandibles in order to correlate mandible thickness with strain patterns from the FEA.

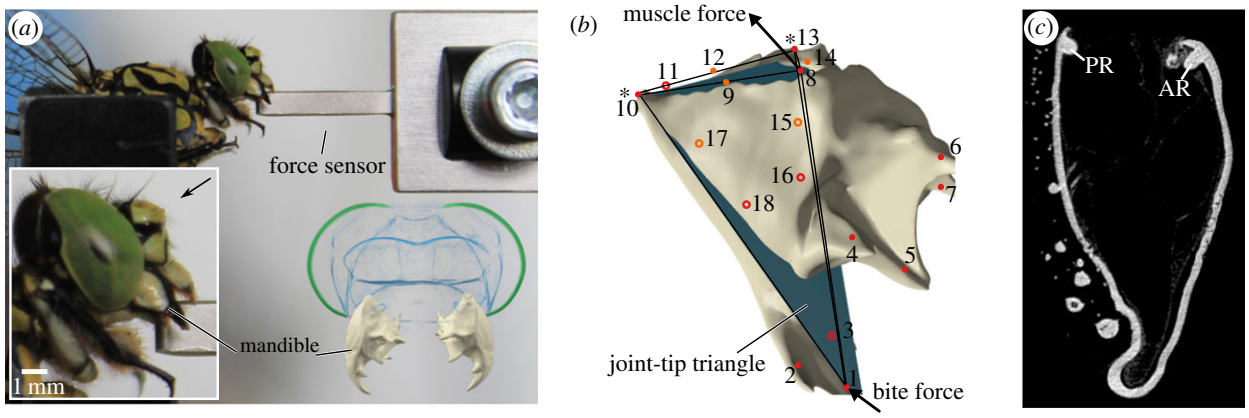


**Figure 1.** (*a*) Set-up for measuring bite forces (lateral view) and principal mandible organization in dragonflies (lower right, frontal view). The black arrow indicates the viewing angle for the three-dimensional model. (*b*) Three-dimensional representation of a dragonfly mandible in lateral view to show the position of the landmarks (red dots) and semi-landmarks (orange), the joints (asterisks), muscle force and bite force and joint-tip triangle (blue). Circles represent landmarks which are on the backside of the mandible. (*c*) Lateral section through the mandible of *Onychogomphus forcipatus* to show the location of the posterior (PR) and anterior (AR) dorsal ridges.

## 2.4. Finite element analysis

We used the FE solver ANSYS (v. 14.5; ANSYS, Inc., USA) for the FEA. The models typically consisted of approximately 175 000 second-order tetrahedral elements (ANSYS type SOLID92). The models were minimally constrained at one node in the *x*-, *y*- and *z*-directions at the anterior and posterior joints, thus allowing free rotation about the joint axis. Nodes over the area of the muscle attachment site were connected individually by LINK180 elements to an additional node in space, so that the direction of the muscle was defined correctly. The measured material properties were not significantly different between the five species measured and between dry ($6.7 \pm 1.2$–$8.9 \pm 0.9$ GPa) and rewetted ($5.4 \pm 0.9$–$9.8 \pm 1.7$ GPa) mandibles. Thus, we used the mean Young's modulus over all measurements for rewetted mandibles (8.8 GPa). We applied a unit load of 1 N to the mandible tips to allow for comparison of strain patterns and thus mouthpart performance in these differently sized mandibles. Bite force measurements for a subset of the species investigated show that mandible bite forces range between 0.3 and 1.8 N depending on the species investigated [22,23]. After the FE solutions were completed, first and third principal strain distributions were displayed on the three-dimensional models, which correspond to the most tensile ($\varepsilon 1$) and most compressive ($\varepsilon 3$) strains at each point of the model. Strain values were also extracted from the middle part of each mandible (the mesal area in posterior view) in order to compare these between species without taking into account local peak strains at the muscle insertions, bite points and joints.

## 2.5. Joint mechanics

To study a potential correlation of mandible joint performance with phylogeny, we used the ANSYS output for the joint reaction forces (JRFs). The two mandible joints and the apical mandible define a triangle (henceforth called the joint-tip triangle; landmarks 1, 10 and 13 in figure 1) where the small side of this triangle defines a virtual axis between the anterior and posterior joint that was used to align the mandibles to each other. The JRF vectors were then imported into Blender and plotted onto these joint-tip triangles to provide a visual representation of the variance in the size and direction of the mandibles' JRFs. Joint-tip triangles were scaled to a length of 1 with respect to the joint axis and aligned along this axis to allow for comparison of the magnitude and direction of the JRFs in three dimensions (electronic supplementary material, three-dimensional model S2). Additionally, we calculated the mechanical advantage (MA) for each mandible. As in vertebrates [32,33], the dicondylous insect mandible can be modelled as a third-order lever. The mandible-closing MA is the ratio between the inner lever arm, which is the distance between the point of application of the input force (here the adductors insertion) and the mandible joint, and the outer lever arm, which is the distance between the mandible joint and the biting point at the tip of the mandible. The MA thus gives a proportion of the muscle force that is transferred to the food item during biting. In a comparative context, the MA can be a useful proxy to assess the biomechanical disparity among taxa, which might be decoupled from the morphological disparity [34,35]. We used the kappa statistic as implemented in the Geomorph package [36,37] to test for potential phylogenetic signal in JRFs and the MA and we calculated phylogenetically independent contrasts to test for correlations between JRFs, size, MA and the biomechanical data represented by the median of the 1000 nodes showing the highest displacements in the median region of each mandible (median of the peak displacements, henceforth MPDs). The phylogeny used, including branch lengths, was obtained from Letsch *et al*. [38] and pruned in R using the Phytools package [39] to represent the biomechanical taxon sampling.

## 2.6. Geometric morphometrics

A series of 18 three-dimensional landmarks, 13 homologous and five semilandmarks, was chosen to represent the three-dimensional shape of each mandible (figure 1 and electronic supplementary material, table S1). All landmarks were exported from Blender (v. 2.77; www.blender.org) from STL models of the mandibles for analysis within the statistics software R [39–42]. After a Procrustes superimposition [43,44] to correct for effects of rotation, translation and size, a principal component analysis (PCA) was performed to investigate the variance associated with the shape variables expressed as principal component scores. Phylogenetic ANOVA, as implemented in Geomorph (procD.pgls), was used to investigate the association of shape (all principal components) with size, MPDs, JRFs and the MA. A multivariate *K*-statistic [36,37] incorporated within the Geomorph package in R was used to account for potential phylogenetic signal in the shape data and in the biomechanical data represented by the MPDs of each mandible. See Adams [36] and Blomberg *et al*. [37] for an estimate of statistical power in relation to sample size. In addition, we tested a potential pairwise correlation of mandible ridges using Pagel's pairwise correlation test of discrete datasets [45] as implemented in the Phytools package for R [39], again taking the phylogeny

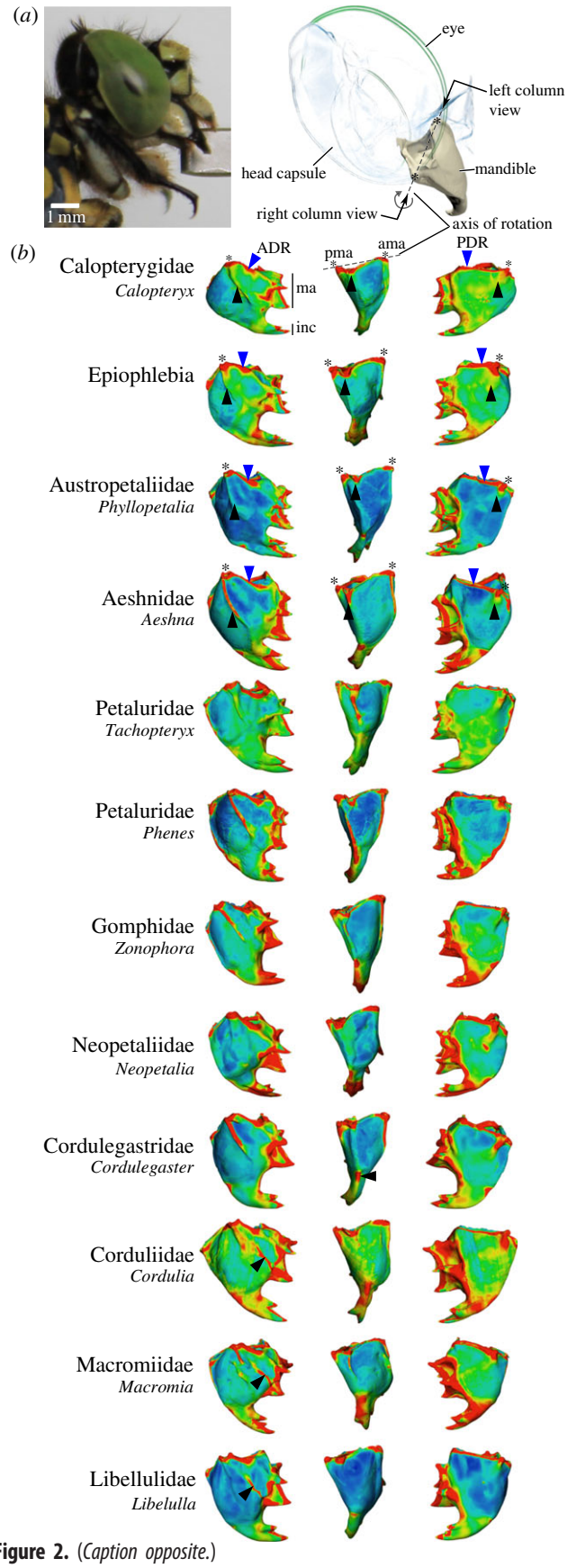


**Figure 2.** (*Caption opposite.*)

published in Letsch *et al*. [38] as a basis. To test whether the mandible ridges showed a phylogenetic signal, we used the phylo.d function in the package Caper, which is able to handle binary coded characters and provides an estimate (*D*) for the phylogenetic signal based on the sum of changes in estimated nodal values of the binary trait tested along the edges of the phylogeny. Additionally, probabilities are calculated for *D* resulting from no phylogenetic structure (phyl.sig), and whether *D* is based on Brownian motion (BM.sig) for each respective character.

**Figure 2.** (*Opposite.*) (*a*) Overview of the head of *Onychogomphus forcipatus* (Gomphidae) in lateral view shows the location of the mandibles within the head and the axis of rotation generated by the anterior and posterior mandibular joints. (*b*) Dimensionless thickness plots for representatives of all dragonfly families. Blue areas represent the thinnest regions, and red areas the thickest. Black and blue arrows indicate ridges and pseudo-ridges mentioned in the text; asterisks indicate the location of joints. Note the appearance of a median ridge in all Libelluloidea studied. Left column, anterior view; middle column, lateral view; right column, posterior view. Left column black arrowhead: anterior acetabular (pseudo)ridge; middle column: lateral ridge; right column: posterior condylar (pseudo)ridge. Blue arrowheads indicate locations of the anterior and posterior dorsal ridges enframing the mandibular orifice. ADR, anterior dorsal ridge; ama, anterior mandibular articulation; inc, incisival area; ma, mesal area; PDR, posterior dorsal ridge; pma, posterior mandibular articulation. Mandible joints are aligned to each other, so that the virtual axis of rotation of the mandible points perpendicular out of the figure. Mandibles not to scale.

# 3. Results

## 3.1. Mandible thickness and the variation of mandible shape and mandible ridges

The principal structure of the dragonfly mandible consists of two ball-and-socket articulations, a strongly sclerotized z-shaped mesal edge with four prominences and usually three distal incisivi (figures 1 and 2). The mandibular orifice is broadly triangular in dorsal view. Thickness plots and external observation show that mandibles of all species have a system of up to six ridges, which are areas of thickened cuticle (figure 2). Among these, the anterior and posterodorsal ones (ADR and PDR, respectively) are present in all species and border the triangular mandibular orifice. The remaining four ridges are variable in location and thickness (figure 2). If present, the anterior acetabular and the posterior condylar ridge (AAR and PCR, respectively) run from the anterior and posterior articulation, respectively, towards the distal incisivi but end blindly well before they reach the distal area of the mandible (taxon dependent). Thickness plots also show that some mandibles, such as those of *Calopteryx*, *Epiophlebia*, *Tachopteryx* and some of the Aeshnidae and Libelluloidea, have anterior ridge-like areas at the same position as the ridges, but, in fact, these are just elevated curved regions only slightly thicker than the surrounding areas (figure 2). We henceforth refer to these structures as pseudo-ridges, in contrast to 'true' ridges that are thickened areas of the cuticle and show a thickness equal to the dorsal ridges. On the posterior side of the mandibles, pseudo-ridges are more frequently encountered, with true ridges only present in *Onychogomphus*, Cordulegastridae and *Neopetalia*. A mesal ridge, which is not visible externally, is present in all Libelluloidea studied (figure 2). A lateral ridge, which originates at the attachment site of the mandibular abductor and extends half way to the apical incisivi in some species, is absent in *Calopteryx*, *Epiophlebia*, *Onychogomphus*, *Oligoaeschna*, *Anotogaster* and the Libellulidae studied. The lateral ridge is strongly developed in Petaluridae and in certain Gomphidae, but weakly developed in the rest of the species.

PCA of mandible shape revealed four major components which together account for 68.38% of the shape variance (figure 3). Phylogenetic signal could be detected in the

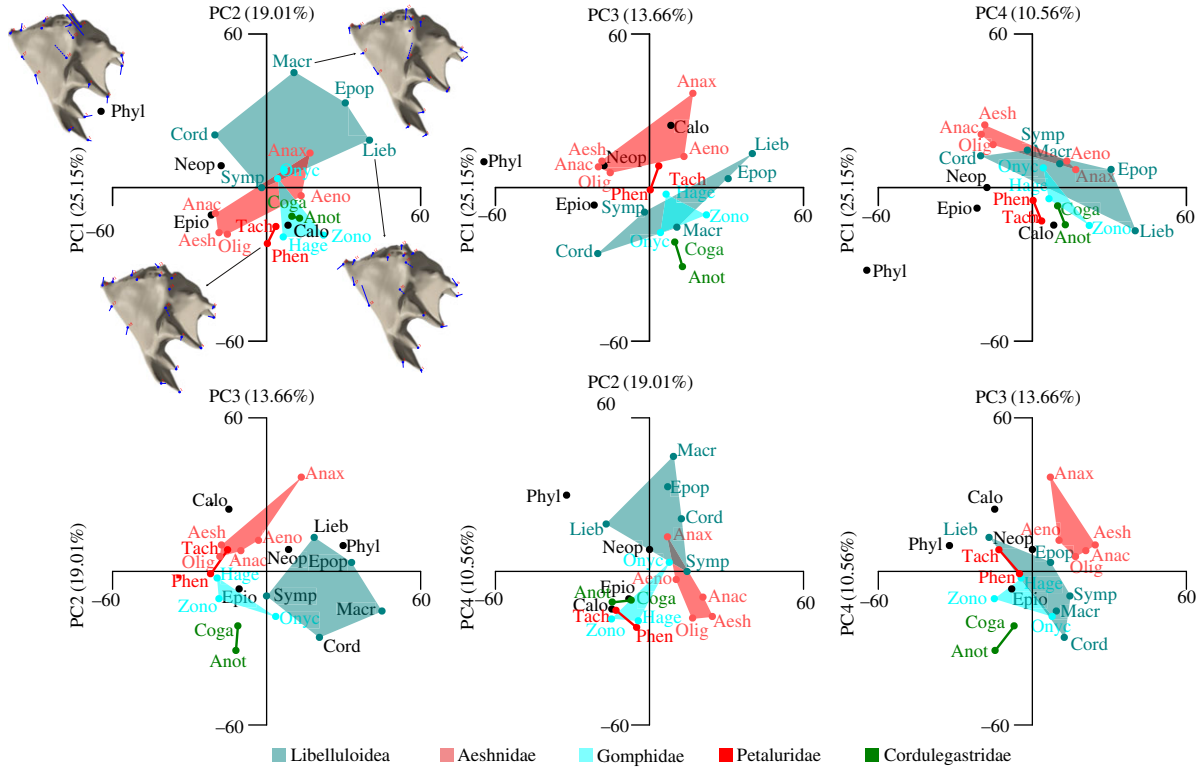


**Figure 3.** PCA showing all combinations of the first four mandible shape components. Data point acronyms are the first four letters of species names (table 1); semi-transparent polygon boxes relate to higher taxa. Mandible images show the plots of the landmark vectors for the extreme mandible shapes of PC1 and PC2.

shape data based on the multivariate *K*-statistic ($K_{mult} = 0.68$, $p = 0.0001$). Taxa that are represented by more than two species such as Libelluloidea, Aeshnidae and Gomphidae are separated from each other in the morphospace of most of the principal component combinations. Petaluridae and Cordulegastridae are also separated in nearly all principal component combinations, but these are only represented by two species each. The austropetaliid *Phylopetalia* is an outlier in nearly all principal component combinations. The plot PC1 versus PC2 (figure 3*a*) shows that the majority of shape variation along PC1 is related to the anterior mandibular joint (landmark 13), the anterior dorsal ridge (L14) and the shape of the anterior acetabular (L15 + 16) and the lateral ridge (L17 + 18). With respect to the consensus shape, the anterior mandibular joint tends to be located more ventrally, while the anterior ridge is located more dorsally at the negative side of PC1. The anterior acetabular ridge is shorter and narrower and the lateral ridge is longer and wider, while at the positive extreme of PC1 the situation is reversed. Along PC2, shape variation again relates to the anterior and posterior joints (L10 + 13) and to the anterior acetabular and the lateral ridge. PC2 mainly codes for the width of the ridges and the joints. Compared with all the above-mentioned structures, the incisivi of the mandibles show only minor shape variations.

Mandible shape is not affected by size, strain (MPDs), JRFs or the MA based on the phylogenetic ANOVA (table 2). With the exception of the median ridge, which is a highly conserved trait among Libelluloidea ($D = -2.66$; phyl.sig = 0.0001; BM.sig = 0.9879), the presence of mandibular ridges does not show phylogenetic signal (table 2). Based on the Pagel [45] correlation test, the mandibular ridges also do not show pairwise correlations to each other (table 2). The ADR and PDR ridges have not been included in this test because they are present in all taxa studied.

## 3.2. Mandible mechanics and the relation to shape and size

All mandibles show high strain directly at their distalmost tips where the bite force was applied, as well as at the attachment site of the large adductor muscle, which is always much thicker than the surrounding areas. Strain patterns differ between the anterior and posterior sides in each species with a generally higher strain ($\varepsilon 1$ and $\varepsilon 3$) on the posterior side. Compressive strains are higher in the lateral regions of the mandibles. A conspicuously thickened but externally indiscernible area lateroventral of the apical incisivi (figures 2 and 4, e.g. Cordulegaster) shows high compressive strain ($\varepsilon 3$) in most of the species. Areas of high tensile strain ($\varepsilon 1$) are located medially between the apical incisivi and the mesal area and, depending on the species, laterally at the mesal base (figure 4 and electronic supplementary material, figure S1).

While the thickness plots show that the presence and configuration of mandibular ridges and pseudo-ridges are highly variable, FEA shows that strain distributions are not always related to ridge presence and location (figure 4 and electronic supplementary material, figure S1). In Aeshnidae, the distribution of the most tensile strains (first principal strain, $\varepsilon 1$) does not overlap with the areas where the anterior acetabular ridge and the lateral ridge are present. Also, there is a low overlap of ridge presence with strain patterns in Libelluloidea. For the most compressive principal strains at each point ($\varepsilon 3$), Libelluloidea show no overlap of strain and structure for the prominent medial and lateral ridges.

In contrast to the thickness plots and strain distributions, box plot graphs of the median and overall variation in principal strain values for all mandibles (figure 5) indicate a family-specific grouping for Libellulidae, Macromiidae and Gomphidae, whereas median strain seems to be more

**Table 2.** Statistical testing framework to test the influence of shape, size, biomechanical determinants and trait presence on each other and to test phylogenetic signal. AAR, anterior acetabular ridge; PCR, posterior condylar ridge; MR, median ridge; LR, lateral ridge, JRF, joint reaction force; MPD, median peak displacement; PIC, phylogenetic independent contrasts. For the definition of JRF angles please refer to figure 6. Italic font indicates significant values.

| | tested traits | *K* | *p*-value |
|---|---|---|---|
| kappa | JRF ($\alpha$) | 0.91 | *0.0127* |
| | JRF ($\beta$) | 0.89 | *0.0185* |
| | JRF ($\gamma$) | 0.57 | 0.2133 |
| | JRF ($\delta$) | 0.55 | 0.2460 |
| | JRF ($\theta$) | 0.26 | 0.9054 |
| | JRF ($\eta$) | 0.29 | 0.8175 |
| | MA | 0.66 | 0.1059 |
| | | $R^2$ | *p*-value |
| Procrustes PGLS | shape versus size | 0.0758 | 0.7373 |
| | shape versus MPDs | 0.0702 | 0.5726 |
| | shape versus JRF ($\alpha$) | 0.0432 | 0.7568 |
| | shape versus JRF ($\beta$) | 0.0424 | 0.5351 |
| | shape versus JRF ($\gamma$) | 0.1430 | 0.2442 |
| | shape versus JRF ($\delta$) | 0.1246 | 0.2523 |
| | shape versus JRF ($\theta$) | 0.0640 | 0.9732 |
| | shape versus JRF ($\eta$) | 0.1070 | 0.8429 |
| | shape versus MA | 0.0762 | 0.0904 |
| PIC | size versus MPDs | 0.0927 | 0.0972 |
| | JRF ($\alpha$) versus MPDs | 0.0005 | 0.9222 |
| | JRF ($\beta$) versus MPDs | 0.0328 | 0.4319 |
| | JRF ($\gamma$) versus MPDs | 0.0598 | 0.2854 |
| | JRF ($\delta$) versus MPDs | 0.0010 | 0.8900 |
| | JRF ($\theta$) versus MPDs | 0.1281 | 0.1112 |
| | JRF ($\eta$) versus MPDs | 0.1021 | 0.1580 |
| | MA versus MPDs | *0.3439* | *0.0052* |
| | JRF ($\alpha$) versus size | 0.0504 | 0.3280 |
| | JRF ($\beta$) versus size | 0.0143 | 0.6063 |
| | JRF ($\gamma$) versus size | 0.0714 | 0.2417 |
| | JRF ($\delta$) versus size | 0.0710 | 0.2431 |
| | JRF ($\theta$) versus size | *0.2739* | *0.0149* |
| | JRF ($\eta$) versus size | *0.3836* | *0.0028* |
| | MA versus size | 0.1625 | 0.0700 |
| | | estimated *D* | no phyl.sig [p] (BM.sig [p]) |
| Phyl. signal in ridge presence | AAR | 0.67 | 0.27 (0.21) |
| | PCR | −0.32 | 0.06 (0.65) |
| | *MR* | *−2.74* | *1 (0.02)* |
| | LR | 0.78 | 0.33 (0.16) |
| | | likelihood ratio | *p*-value |
| pairwise correlation of ridges | AAR \| PCR | 2.1031 | 0.7168 |
| | AAR \| MR | 0.9736 | 0.9138 |
| | AAR \| LR | 5.8201 | 0.2138 |
| | PCR \| MR | 2.6425 | 0.4742 |
| | PCR \| LR | 6.0530 | 0.1945 |
| | MR \| LR | 1.4166 | 0.8413 |

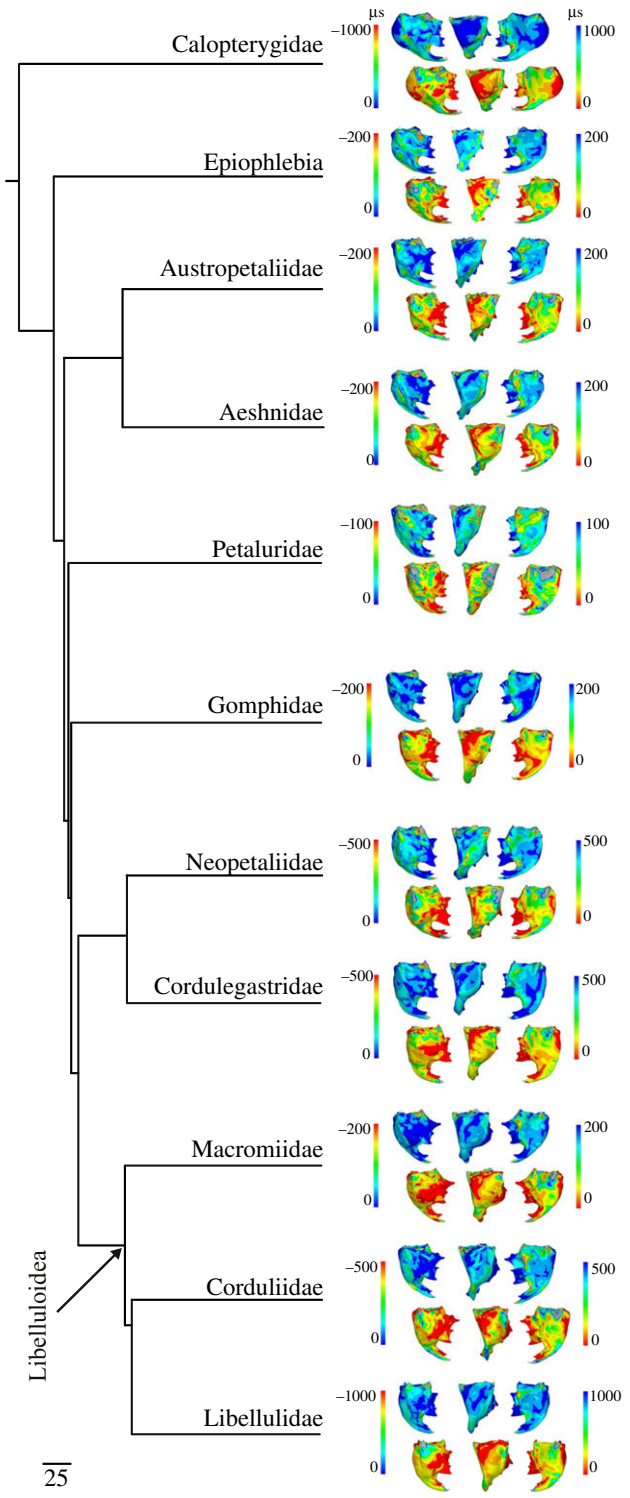


**Figure 4.** First ($\varepsilon$1) and third ($\varepsilon$3) principal strain distributions in the mandibles mapped onto the most recent comprehensive phylogeny provided for dragonflies (Anisoptera; Letsch *et al*. [38]). Left column, anterior view; middle column, lateromedial view; right column, posterior view; $\varepsilon$1 upper row with left-hand colour key; $\varepsilon$3 lower row with right-hand colour key. A unit force of 1 N was used for all species. Only exemplary mandibles are shown; for a full overview of strain patterns per species please refer to the electronic supplementary material, figure S1.

variable in Cordulegastridae, Petaluridae and Aeshnidae. Although the application of a unit force of 1 N to each mandible facilitates an easier comparison of strain patterns, for those species where bite forces could be measured [22,23] the box plots are also scaled in order to derive an estimate of the *in vivo* strain values. Results show that *Sympetrum* most likely experiences lower *in vivo* strain, whereas

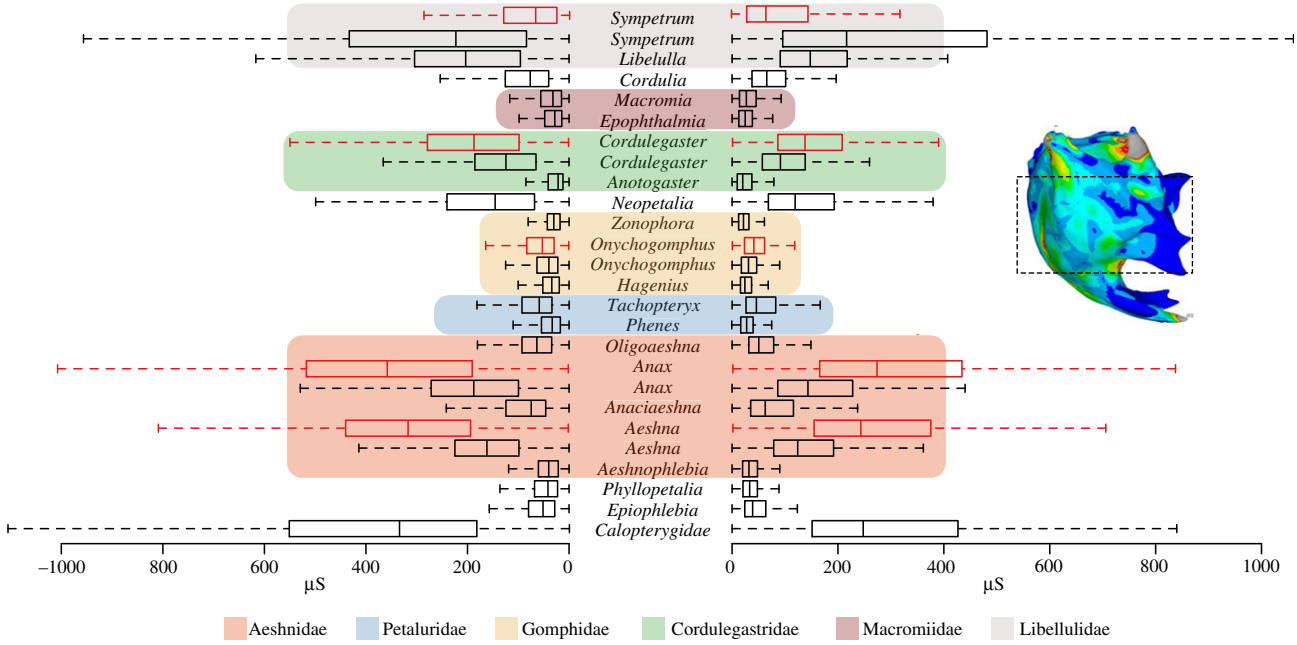


**Figure 5.** Boxplots show the range of first ($\varepsilon 1$, right side) and third ($\varepsilon 3$, left side) principal strain distributions for the middle part of each mandible (see sample insert) of the full species set at a unit force of 1 N. Note that the highlighted middle part was used to calculate the median of the 1000 nodes showing the highest displacements (MPDs). Coloured boxes indicate families, red boxplots show ranges of $\varepsilon 1$ and $\varepsilon 3$ after rescaling according to the bite force measurements. Please refer to the electronic supplementary material, figure S2, for an overview of strain ranges including outliers.

*Cordulegaster*, *Onychogomphus*, *Anax* and *Aeshna* have higher *in vivo* values, in the case of *Anax* and *Aeshna* nearly twice as high. Phylogenetic signal could not be detected in the strain data represented by the MPDs of each mandible based on the kappa statistic ($K = 0.50$, $p = 0.3289$).

Analysis of the joint mechanics expressed in terms of JRF vectors shows a similar family-specific pattern as in the box plots of strain distributions for the angle between anterior and posterior JRFs in posterior view ($\alpha$, figure 6), whereas such a pattern is not apparent for the rest of the measured angles ($\beta - \eta$; figure 6). The JRF angles $\alpha$ and $\beta$ show phylogenetic signal ($\alpha$: $K = 0.91$, $p = 0.01$; $\beta$: $K = 0.89$, $p = 0.02$; table 2), whereas the distribution of the mandibular advantage does not show significant phylogenetic signal. JRF angles $\theta$ and $\eta$ (the lateral 'spread' of posterior and anterior JRF vectors, see figure 6) show a correlation with mandible size (table 2). The mean value of the mandible-closing MA over all species is $0.38 \pm 0.017$ with the lowest values (0.35) shown by species such as *Neopetalia* and *Phyllopetalia*. The highest MAs (0.41) are shown by *Aeshna* and *Sympetrum*. The MA is correlated with MPDs, whereas the JRFs do not show such a correlation.

# 4. Discussion

## 4.1. The interplay of shape, biomechanics, phylogeny and size in dragonfly mandibles

Surprisingly few studies have tried to quantify mandible shape and biomechanics in insects [7,8,11,13], and there are no studies combining biomechanical determinants with shape characteristics in a phylogenetic framework. Our results obtained from the three-dimensional shape analysis and FEA of mandibles belonging to 21 different species of dragonflies suggest a rather complicated interplay of shape, biomechanics and phylogeny in taxa with uniform feeding habits. Mandible shape shows phylogenetic signal and a $K_{mult}$ value lower than 1 suggests that taxa are more similar than expected under a Brownian motion model of evolution. This effect could also be detected for some biomechanical determinants (table 2), specifically for the angle between anterior and posterior JRFs in anterior view (JRF $\alpha$) and the direction of the posterior JRF in lateral view (JRF $\beta$). A possible explanation is selection of the above-mentioned biomechanical factors to reach a certain mandible performance which, in turn, requires convergent evolution of a combination of shape variables supporting the required mechanical performance. In line with this suggestion is the correlation of the MA with MPDs (table 2), because the MA is solely a shape-dependent index of mandible performance. Furthermore, the results suggest that size effects only play a minor role for specific JRF angles although size differences are more than twofold (table 1).

The lacking phylogenetic signal in MPDs despite such a signal in JRFs could be due to the averaging of strain results over a wide shape area. For a more detailed account, it would be necessary to compare different strain *patterns* with each other and assess the phylogenetic signal in pattern variation. However, such an approach is obviously difficult to realize because this would require an exact structural similarity of each mandible so that an element-by-element comparison of strain values is possible.

Phylogenetic signal in a combination of shape and functional parameters has not been assessed so far in insects but is a well-known phenomenon in vertebrates [46–51]. It was shown that multiple processes can in fact produce patterns of phenotypic diversification similar to phylogenetic signal [36,37,50,52,53]. In those instances where biomechanical determinants were additionally measured, the decisive influence of biomechanics on shape and vice versa was apparent [4,54–56], and in some instances superposing phylogenetic signal [55]. Overall, our results suggest that the disparity in the phenotype is lower than expected under Brownian motion and

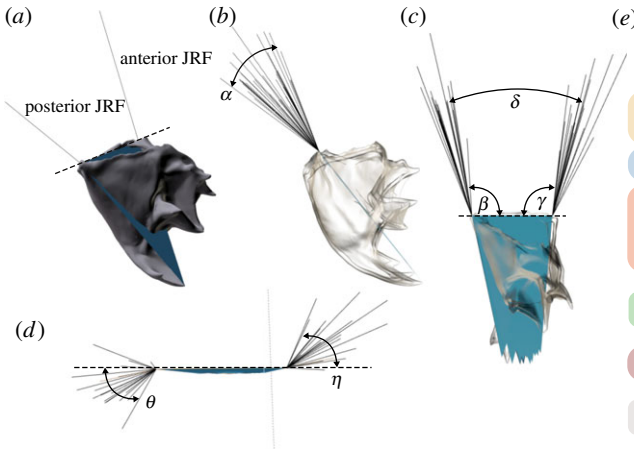


(e)

| species | (α) | (β) | (γ) | (δ) | (θ) | (η) | \|θ\|+\|η\| | MA |
|---|---|---|---|---|---|---|---|---|
| total range over all species | 41.5 | | | | 90.41 | 110.96 | | |
| *Calopteryx virgo* | 10.7 | 117.9 | 102.4 | 40.3 | 15.67 | 13.59 | 29.27 | 0.39 |
| *Epiophlebia superstes* | 14.3 | 104.3 | 107.9 | 32.2 | 34.30 | 6.66 | 40.96 | 0.36 |
| *Onychogomphus forcipatus* | 23.3 | 98.0 | 106.7 | 24.7 | 21.37 | 65.40 | 86.77 | 0.40 |
| *Hagenius brevistylus* | 7.0 | 103.1 | 108.0 | 31.1 | 26.26 | –9.25 | 35.50 | 0.38 |
| *Zonophora batesi* | 7.8 | 103.0 | 111.2 | 34.2 | 16.56 | 4.16 | 20.71 | 0.39 |
| *Phenes raptor* | 6.6 | 103.1 | 106.9 | 30.0 | 14.73 | 7.23 | 21.96 | 0.38 |
| *Tachopteryx thoreyi* | 6.9 | 115.1 | 102.6 | 37.6 | –15.52 | 21.70 | 37.22 | 0.37 |
| *Anax imperator* | 24.9 | 97.4 | 97.9 | 15.3 | 39.80 | 67.67 | 107.46 | 0.38 |
| *Aeshna mixta* | 19.8 | 99.8 | 106.8 | 26.6 | 26.73 | 49.03 | 75.76 | 0.41 |
| *Aeshnophlebia anisoptera* | 19.3 | 102.5 | 106.4 | 28.9 | 29.65 | 37.72 | 67.37 | 0.38 |
| *Anaciaeshna isoceles* | 15.6 | 105.6 | 105.9 | 31.5 | –0.66 | 45.23 | 45.90 | 0.38 |
| *Oligoaeschna pryeri* | 17.4 | 96.3 | 106.7 | 23.1 | 34.14 | 40.64 | 74.77 | 0.40 |
| *Phyllopetalia apicalis* | 16.3 | 110.9 | 108.8 | 39.7 | 8.13 | 32.48 | 40.61 | 0.35 |
| *Anotogaster sieboldii* | 22.9 | 103.1 | 105.5 | 28.5 | –31.57 | –43.31 | 74.87 | 0.39 |
| *Cordulegaster bidentata* | 17.8 | 100.7 | 101.2 | 21.9 | 41.39 | 34.72 | 76.11 | 0.39 |
| *Neopetalia punctata* | 26.3 | 104.1 | 104.7 | 28.7 | 32.87 | 49.92 | 82.79 | 0.35 |
| *Macromia taeniolata* | 9.2 | 105.9 | 99.5 | 25.4 | –9.66 | 34.04 | 43.70 | 0.38 |
| *Epophthalmia elegans* | 7.3 | 106.5 | 93.5 | 20.0 | –31.44 | 29.51 | 60.95 | 0.37 |
| *Cordulia aenea* | 19.9 | 110.2 | 98.5 | 28.7 | 47.59 | 26.58 | 74.16 | 0.37 |
| *Sympetrum vulgatum* | 26.4 | 119.6 | 95.4 | 35.01 | –1.39 | 41.44 | 42.83 | 0.41 |
| *Libellula depressa* | 25.4 | 105.9 | 99.2 | 25.1 | 59.12 | 31.94 | 91.05 | 0.38 |

Aeshnidae Petaluridae Gomphidae
Cordulegastridae Macromiidae Libellulidae

**Figure 6.** The range of JRF vectors for anisopteran mandibles. (*a–d*) Visual overview of measured angles. The dashed line shows the virtual joint axis around which the mandible rotates during biting. All mandibles were aligned to this axis for comparison of JRFs. (*b*) The range of aligned JRF vectors in posterior view, (*c*) in lateral view and (*d*) in ventral view (seen along the triangular plane indicated in (*a*)). (*e*) Overview of the measured angles; coloured boxes indicate families with the same colour code as in figure 3. See the electronic supplementary material, model S3, for fully interactive three-dimensional models of joint-tip triangles.

biomechanics do not follow this pattern. In fact, our results suggest that the biomechanical determinants measured here seem to be decoupled from the shape variation at this taxonomic level.

The MA values measured for dragonflies are in the range of the most advantageous lever ratios (i.e. the most joint-near-tooth row or advantageous muscle insertions) measured for vertebrates [57–59] and the American cockroach [8]. This relative uniformity of MA in distantly related taxa such as cockroaches and dragonflies suggests that the observed differences in biomechanical determinants and shape lead to a comparably narrow overall mandible performance space represented by the MA. Taking into account the above-mentioned decoupling of mechanics from shape, we suggest that this narrow MA range might be the effect of a 'many-to-one mapping' of different forms to the same function [46,47,60], leading to the same functional performance space. However, more insect lineages need to be studied to corroborate this notion.

## 4.2. Biomechanical characteristics of dragonfly mandibles

Generally, higher strains are located around bite points and muscle attachments, as observed in similar FE studies of vertebrate crania and mandibles [61–63] and insect mandibles [64,65]. Another general area of high strain is located in all mandibles between the apical incisival area and the z-shaped mesal edge. Although it is currently not possible to reliably compare and test strain *patterns* against shape, we suggest that this correspondence in overall strain distribution is most probably related to the similarity in overall mandible morphology and applied loadings and constraints. Visual examination of the detailed strain patterns at the lateral parts of the mandibles, however, shows that the local strain distributions are highly variable. For example, strain is not correlated with the presence of ridges in most of the Aeshnidae and Libelluloidea studied. A similar phenomenon of non-correspondence of ridges with strain could be observed in vertebrates where the function of the brow ridge (supraorbital torus) in primates has been the subject of much debate, with studies showing that brow ridges are indeed lightly loaded during normal biting [66].

We applied a unit bite force (1 N) to all mandibles, because actual bite force values are not known for many of the rare species we investigated here. It should be remembered that absolute bite forces are not relevant for the purpose of this study, because strain patterns are of course independent of the absolute magnitude values of bite forces. On the other hand, the application of a standardized bite force allows an easy comparison of the relative mandible efficiencies. Our results suggest that the mandible shapes of Gomphidae and Macromiidae are among the most efficient in terms of principal strain distribution (figure 5). Taking into account the bite forces which could be measured [22,23], the observed strain distributions for a unit force load are most likely an overestimation of *in vivo* strain in the smaller Libellulidae and *Calopteryx*, whereas they are an underestimation for the larger species within Aeshnidae, Cordulegastridae, Macromiidae, Petaluridae and to a lesser extent Gomphidae (figure 4). As in vertebrates, absolute bite force in dragonflies probably depends on head geometry, which also determines the characteristics of the lever arm system, e.g. adductor muscle mass and muscle architecture such as pennation and fibre length [59,67–69]. In contrast to vertebrates, however, an allometric scaling of bite force was not found for the species investigated here [22], which is also indicated by the lacking relationship between size and MPDs (table 2). The middle-sized gomphid *Onychogomphus forcipatus* showed an even higher bite force than one of the largest European dragonflies, *Cordulegaster bidentata* [22]. Future studies, taking into account more insect lineages, have to elucidate whether a non-allometric scaling of absolute bite forces is a more widespread phenomenon among insects.

## 4.3. A wider evolutionary perspective on mandible mechanics in basal insects

Strain levels at the posterior side of the mandibles are consistently higher than on the anterior sides (figure 3), which is most probably related to the posteriorly directed force vector of the main mandibular adductor muscle.

Interestingly, at the same time, the condyle-like mandibular part of the posterior joint shows a remarkable structural similarity within ectognathous insects (bristletails, silverfish and winged insects) compared with the anterior joint, although the food spectrum is highly variable [21,70–73]. Bristletails feed on algae, lichens and mosses, silverfish consume organic detritus and mayflies mainly feed on algae and detritus, with predacious species as the exception. A potential reason for this relative structural constancy in the posterior condyle may be the higher loadings this structure experiences compared with the anterior joint during biting. The structural change of the posterior mandibular joint during the evolution of the insect mandible might be restricted owing to functional demands, as was suggested for structures in other animal groups [2,4,56]. In contrast, strain levels at the anterior mandibular joint are lower and this joint is at the same time structurally more variable throughout the early split ectognathous insects. Bristletails show a loose contact with the head capsule at the anterior part of the mandible [73], silverfish have a pincer-like structure guiding the mandible during movement in one direction [72,74], whereas mayflies show an anterior articulation complex in fact composed of two mandible–head contacts [75]. Finally, dragonflies and the majority of other chewing–biting insects, e.g. Polyneoptera, show the typical ball-and-socket joint type at the anterior side of the mandible. This structural variability in the anterior mandible joint during early insect evolution might have been possible owing to the lower loadings experienced so that the constraining effect of biomechanics on shape was less. However, biomechanical data for bristletails, silverfish and mayflies will be needed to test these ideas in an evolutive framework. Because sensitivity studies have proven the significant negative impact of simplifications in geometry and boundary conditions for vertebrates [67,76–87], much more experimental data on insect mouthpart mechanics are needed to quantitatively assess patterns of biomechanical evolution across insects.

Authors' contributions. A.B. and M.J.F. conceived and designed the study. A.B. and A.P. did the SR-μCT, A.B. carried out all other experiments and simulations. H.S. helped with the nano-indentations, H.D. helped with the FEA. A.B. analysed and interpreted the data. All authors read and corrected earlier versions of the manuscript and approved the final version.

Competing interests. We have no competing interests.

Funding. The financial support of the Deutsches Elektronen Synchrotron (I-20120065) and the Paul-Scherrer Institut (20150464; synchrotron experiments) is gratefully acknowledged. A.B. was supported by a research fellowship from the Deutsche Forschungsgemeinschaft (BL 1355/1-1). H.D. was supported through BBSRC grant no. BB/M008525/1.

Acknowledgements. We thank Anke Schmitz for help during the nano-indentation experiments and Felix Beckmann, Karen Meusemann, Björn M. von Reumont and Susanne Düngelhoef for help during the SR-μCT experiments. Sina David and Johannes Funken (German Sport University, Cologne, Germany) are sincerely thanked for their help during bite force measurements. Manon Galland (currently University College Dublin, Dublin, Ireland) helped with the geometric morphometric analysis workflow. Bernhard Misof and Anthony Herrel are thanked for valuable discussions during the preparation of this manuscript. We furthermore thank the very constructive comments of four reviewers on an earlier version of the manuscript.

## References

1. Gould SJ. 1966 Allometry and size in ontogeny and phylogeny. *Biol. Rev.* **41**, 587–638. (doi:10.1111/j.1469-185X.1966.tb01624.x)
2. Smith JM, Burian R, Kauffman S, Alberch P, Campbell J, Goodwin B, Lande R, Raup D, Wolpert L. 1985 Developmental Mountain Lake Conference: a perspective from the Mountain Lake Conference on development and evolution. *Q. Rev. Biol.* **60**, 265–287. (doi:10.1086/414425)
3. Gans C. 1988 On phylogenetic constraints. *Acta Morphol. Neerl. Scand.* **27**, 133–138.
4. Arnold SJ. 1992 Constraints on phenotypic evolution. *Am. Nat.* **140**, S85–S107. (doi:10.1086/285398)
5. Paul J, Gronenberg W. 1999 Optimizing force and velocity: mandible muscle fibre attachments in ants. *J. Exp. Biol.* **202**, 797–808.
6. Goyens J, Dirckx J, Dierick M, Hoorebeke LV, Aerts P. 2014 Biomechanical determinants of bite force dimorphism in *Cyclommatus metallifer* stag beetles. *J. Exp. Biol.* **217**, 1065–1071. (doi:10.1242/jeb.091744)
7. Schmitt C, Rack A, Betz O. 2014 Analyses of the mouthpart kinematics in *Periplaneta americana* (Blattodea, Blattidae) by using synchrotron-based X-ray cineradiography. *J. Exp. Biol.* **217**, 3095–3107. (doi:10.1242/jeb.092742)
8. Weihmann T, Reinhardt L, Weißing K, Siebert T, Wipfler B. 2015 Fast and powerful: biomechanics and bite forces of the mandibles in the American cockroach *Periplaneta americana*. *PLoS ONE* **10**, e0141226. (doi:10.1371/journal.pone.0141226)
9. Josephson RK, Young D. 1987 Fiber ultrastructure and contraction kinetics in insect fast muscles. *Am. Zool.* **27**, 991–1000. (doi:10.1093/icb/27.4.991)
10. Gronenberg W, Paul J, Just S, Hölldobler B. 1997 Mandible muscle fibers in ants: fast or powerful? *Cell Tissue Res.* **289**, 347–361. (doi:10.1007/s004410050882)
11. Paul J. 2001 Mandible movements in ants. *Comp. Biochem. Physiol. A. Mol. Integr. Physiol.* **131**, 7–20. (doi:10.1016/S1095-6433(01)00458-5)
12. Paul J, Gronenberg W. 2002 Motor control of the mandible closer muscle in ants. *J. Insect Physiol.* **48**, 255–267. (doi:10.1016/S0022-1910(01)00171-8)
13. Gorb S, Beutel RG. 2000 Head-capsule design and mandible control in beetle larvae: a three-dimensional approach. *J. Morphol.* **244**, 1–14. (doi:10.1002/(SICI)1097-4687(200004)244:1<1::AID-JMOR1>3.0.CO;2-E)
14. Smith TR, Capinera JL. 2005 Mandibular morphology of some Floridian grasshoppers (Orthoptera: Acrididae). *Fla. Entomol.* **88**, 204–207. (doi:10.1653/0015-4040(2005)088[0204:MMOSFG]2.0.CO;2)
15. Matsuda R. 1965 Morphology and evolution of the insect head. *Mem. Am. Entomol. Inst.* **1**, 1–334.
16. Labandeira CC. 1997 Insect mouthparts: ascertaining the paleobiology of insect feeding strategies. *Annu. Rev. Ecol. Syst.* **28**, 153–193. (doi:10.1146/annurev.ecolsys.28.1.153)
17. Grimaldi D, Engel MS. 2005 *Evolution of the Insects*. Cambridge, UK: Cambridge University Press.
18. Corbet PS. 1999 *Dragonflies: behaviour and ecology of Odonata*. Colchester, UK: Harley Books.
19. Tillyard RJ. 1917 *The biology of dragonflies* (*Odonata or Paraneuroptera*). Cambridge, UK: Cambridge University Press.
20. Asahina S. 1954 *Morphological study of a relic dragonfly Epiophlebia superstes Selys* (*Odonata, Anisozygoptera*). Tokyo, Japan: Japan Society for the Promotion of Science.
21. Beutel RG, Friedrich F, Ge SQ, Yang XK. 2014 *Insect morphology and phylogeny*. Berlin, Germany: De Gruyter.
22. David S, Funken J, Potthast W, Blanke A. 2016 Musculoskeletal modelling under an evolutionary perspective: deciphering the role of single muscle regions in closely related insects. *J. R. Soc. Interface* **13**, 20160675. (doi:10.1098/rsif.2016.0675)
23. David S, Funken J, Potthast W, Blanke A. 2016 Musculoskeletal modeling of the dragonfly

mandible system as an aid to understanding the role of single muscles in an evolutionary context. *J. Exp. Biol*. **219**, 1041–1049. (doi:10.1242/jeb.132399)

24. Klocke D, Schmitz H. 2011 Water as a major modulator of the mechanical properties of insect cuticle. *Acta Biomater*. **7**, 2935–2942. (doi:10.1016/j.actbio.2011.04.004)
25. Klocke D, Schmitz H. 2012 Material properties of photomechanical infrared receptors in pyrophilous Melanophila beetles and Aradus bugs. *Acta Biomater*. **8**, 3392–3399. (doi:10.1016/j.actbio.2012.05.020)
26. Oliver WC, Pharr GM. 1992 An improved technique for determining hardness and elastic modulus using load and displacement sensing indentation experiments. *J. Mater. Res*. **7**, 1564–1583. (doi:10.1557/JMR.1992.1564)
27. Romeis B. 1989 *Mikroskopische Technik*. Munich, Germany: Urban & Schwarzenberg.
28. Beckmann F, Herzen J, Haibel A, Müller B, Schreyer A. 2008 High density resolution in synchrotron-radiation-based attenuation-contrast microtomography. *Proc. SPIE* **7078**, 70781D-13. (doi:10.1117/12.794617)
29. Stampanoni M, Marone F, Modregger P, Pinzer B, Thüring T, Vila-Comamala J, David C, Mokso R. 2010 Tomographic hard X-ray phase contrast micro- and nano-imaging at TOMCAT. *AIP Conf. Proc*. **1266**, 13–17. (doi:10.1063/1.3478189)
30. Blanke A, Greve C, Mokso R, Beckmann F, Misof B. 2013 An updated phylogeny of Anisoptera including formal convergence analysis of morphological characters. *Syst. Entomol*. **38**, 474–490. (doi:10.1111/syen.12012)
31. Yushkevich PA, Piven J, Hazlett HC, Smith RG, Ho S, Gee JC, Gerig G. 2006 User-guided 3D active contour segmentation of anatomical structures: significantly improved efficiency and reliability. *Neuroimage* **31**, 1116–1128. (doi:10.1016/j.neuroimage.2006.01.015)
32. Westneat MW. 1995 Feeding, function, and phylogeny: analysis of historical biomechanics in labrid fishes using comparative methods. *Syst. Biol*. **44**, 361–383. (doi:10.1093/sysbio/44.3.361)
33. Anderson PSL, Friedman M, Brazeau MD, Rayfield EJ. 2011 Initial radiation of jaws demonstrated stability despite faunal and environmental change. *Nature* **476**, 206–209. (doi:10.1038/nature10207)
34. Hulsey CD, Wainwright PC. 2002 Projecting mechanics into morphospace: disparity in the feeding system of labrid fishes. *Proc. Biol. Sci*. **269**, 317–326. (doi:10.1098/rspb.2001.1874)
35. Anderson PSL. 2009 Biomechanics, functional patterns, and disparity in Late Devonian arthrodires. *Paleobiology* **35**, 321–342. (doi:10.1666/0094-8373-35.3.321)
36. Adams DC. 2014 A generalized K statistic for estimating phylogenetic signal from shape and other high-dimensional multivariate data. *Syst. Biol*. **63**, 685–697. (doi:10.1093/sysbio/syu030)
37. Blomberg SP, Garland T, Ives AR. 2003 Testing for phylogenetic signal in comparative data: behavioral traits are more labile. *Evolution* **57**, 717–745. (doi:10.1111/j.0014-3820.2003.tb00285.x)
38. Letsch H, Gottsberger B, Ware JL. 2016 Not going with the flow: a comprehensive time-calibrated phylogeny of dragonflies (Anisoptera: Odonata: Insecta) provides evidence for the role of lentic habitats on diversification. *Mol. Ecol*. **25**, 1340–1353. (doi:10.1111/mec.13562)
39. Revell LJ. 2012 phytools: an R package for phylogenetic comparative biology (and other things). *Methods Ecol. Evol*. **3**, 217–223. (doi:10.1111/j.2041-210X.2011.00169.x)
40. Adams DC, Otárola-Castillo E. 2013 geomorph: an R package for the collection and analysis of geometric morphometric shape data. *Methods Ecol. Evol*. **4**, 393–399. (doi:10.1111/2041-210X.12035)
41. Dryden IL. 2015 Shapes package, v. 11-11. *Vienna, Austria/l R* Foundation.
42. Popescu A-A, Huber KT, Paradis E. 2012 ape 3.0: new tools for distance-based phylogenetics and evolutionary analysis in R. *Bioinformatics* (*Oxford Engl*.) **28**, 1536–1537. (doi:10.1093/bioinformatics/bts184)
43. Gower JC. 1975 Generalized procrustes analysis. *Psychometrika* **40**, 33–51. (doi:10.1007/BF02291478)
44. Rohlf FJ, Slice D. 1990 Extensions of the procrustes method for the optimal superimposition of landmarks. *Syst. Zool*. **39**, 40–59. (doi:10.2307/2992207)
45. Pagel M. 1994 Detecting correlated evolution on phylogenies: a general method for the comparative analysis of discrete characters. *Proc. R. Soc. Lond. B* **255**, 37–45. (doi:10.1098/rspb.1994.0006)
46. Alfaro ME, Bolnick DI, Wainwright PC. 2005 Evolutionary consequences of many-to-one mapping of jaw morphology to mechanics in labrid fishes. *Am. Nat*. **165**, E140–E154. (doi:10.1086/429564)
47. Wainwright PC, Alfaro ME, Bolnick DI, Hulsey CD. 2005 Many-to-one mapping of form to function: a general principle in organismal design? *Integr. Comp. Biol*. **45**, 256–262. (doi:10.1093/icb/45.2.256)
48. Rezende EL, Diniz-Filho JAF. 2012 Phylogenetic analyses: comparing species to infer adaptations and physiological mechanisms. *Compr. Physiol*. **2**, 639–674. (doi:10.1002/cphy.c100079)
49. Rheindt FE, Grafe TU, Abouheif E. 2004 Rapidly evolving traits and the comparative method: how important is testing for phylogenetic signal? *Evol. Ecol. Res*. **6**, 377–396.
50. Revell LJ, Harmon LJ, Collar DC. 2008 Phylogenetic signal, evolutionary process, and rate. *Syst. Biol*. **57**, 591–601. (doi:10.1080/10635150802302427)
51. Segall M, Cornette R, Fabre A-C, Godoy-Diana R, Herrel A. 2016 Does aquatic foraging impact head shape evolution in snakes?. *Proc. R. Soc. B* **283**, 20161645. (doi:10.1098/rspb.2016.1645)
52. Ackerly D. 2009 Conservatism and diversification of plant functional traits: evolutionary rates versus phylogenetic signal. *Proc. Natl Acad. Sci. USA* **106**, 19 699–19 706. (doi:10.1073/pnas.0901635106)
53. Pennell MW, Harmon LJ. 2013 An integrative view of phylogenetic comparative methods: connections to population genetics, community ecology, and paleobiology. *Ann. NY Acad. Sci*. **1289**, 90–105. (doi:10.1111/nyas.12157)
54. Levinton JS, Allen BJ. 2005 The paradox of the weakening combatant: trade-off between closing force and gripping speed in a sexually selected combat structure. *Funct. Ecol*. **19**, 159–165. (doi:10.1111/j.0269-8463.2005.00968.x)
55. Piras P, Maiorino L, Teresi L, Meloro C, Lucci F, Kotsakis T, Raia P. 2013 Bite of the cats: relationships between functional integration and mechanical performance as revealed by mandible geometry. *Syst. Biol*. **62**, 878–900. (doi:10.1093/sysbio/syt053)
56. Konuma J, Chiba S. 2007 Trade-offs between force and fit: extreme morphologies associated with feeding behavior in carabid beetles. *Am. Nat*. **170**, 90–100. (doi:10.1086/518182)
57. Sakamoto M. 2010 Jaw biomechanics and the evolution of biting performance in theropod dinosaurs. *Proc. R. Soc. B* **277**, 3327–3333. (doi:10.1098/rspb.2010.0794)
58. Dutel H, Herbin M, Clément G, Herrel A. 2015 Bite force in the extant coelacanth latimeria: the role of the intracranial joint and the basicranial muscle. *Curr. Biol*. **25**, 1228–1233. (doi:10.1016/j.cub.2015.02.076)
59. McIntosh AF, Cox PG. 2016 Functional implications of craniomandibular morphology in African mole-rats (Rodentia: Bathyergidae). *Biol. J. Linn. Soc*. **117**, 447–462. (doi:10.1111/bij.12691)
60. Alfaro ME, Bolnick DI, Wainwright PC. 2004 Evolutionary dynamics of complex biomechanical systems: an example using the four-bar mechanism. *Evolution* **58**, 495–503. (doi:10.1111/j.0014-3820.2004.tb01673.x)
61. Fitton LC, Shi JF, Fagan MJ, O'Higgins P. 2012 Masticatory loadings and cranial deformation in *Macaca fascicularis*: a finite element analysis sensitivity study. *J. Anat*. **221**, 55–68. (doi:10.1111/j.1469-7580.2012.01516.x)
62. Curtis N, Jones MEH, Evans SE, O'Higgins P, Fagan MJ. 2013 Cranial sutures work collectively to distribute strain throughout the reptile skull. *J. R. Soc. Interface* **10**, 20130442. (doi:10.1098/rsif.2013.0442)
63. Gill PG, Purnell MA, Crumpton N, Brown KR, Gostling NJ, Stampanoni M, Rayfield EJ. 2014 Dietary specializations and diversity in feeding ecology of the earliest stem mammals. *Nature* **512**, 303–305. (doi:10.1038/nature13622)
64. Hörnschemeyer T, Bond J, Young PG. 2013 Analysis of the functional morphology of mouthparts of the beetle *Priacma serrata*, and a discussion of possible food sources. *J. Insect Sci*. **13**, 1–14. (doi:10.1673/031.013.12601)
65. Goyens J, Soons J, Aerts P, Dirckx J. 2014 Finite-element modelling reveals force modulation of jaw adductors in stag beetles. *J. R. Soc. Interface* **11**, 20140908. (doi:10.1098/rsif.2014.0908)

66. Kupczik K, Dobson CA, Crompton RH, Phillips R, Oxnard CE, Fagan MJ, O'Higgins P. 2009 Masticatory loading and bone adaptation in the supraorbital torus of developing macaques. *Am. J. Phys. Anthropol*. **139**, 193–203. (doi:10.1002/ajpa.20972)
67. Gröning F, Jones MEH, Curtis N, Herrel A, O'Higgins P, Evans SE, Fagan MJ. 2013 The importance of accurate muscle modelling for biomechanical analyses: a case study with a lizard skull. *J. R. Soc. Interface* **10**, 20130216. (doi:10.1098/rsif.2013.0216)
68. Cox PG, Baverstock H. 2015 Masticatory muscle anatomy and feeding efficiency of the American beaver, *Castor canadensis* (Rodentia, Castoridae). *J. Mamm. Evol*. **23**, 191–200. (doi:10.1007/s10914-015-9306-9)
69. Ledogar JA *et al.* 2016 Mechanical evidence that Australopithecus sediba was limited in its ability to eat hard foods. *Nat. Commun*. **7**, 10596. (doi:10.1038/ncomms10596)
70. Engel MS, Grimaldi DA. 2004 New light shed on the oldest insect. *Nature* **427**, 627–630. (doi:10.1038/nature02291)
71. Blanke A, Wipfler B, Letsch H, Koch M, Beckmann F, Beutel R, Misof B. 2012 Revival of Palaeoptera—head characters support a monophyletic origin of Odonata and Ephemeroptera (Insecta). *Cladistics* **28**, 560–581. (doi:10.1111/j.1096-0031.2012.00405.x)
72. Blanke A, Koch M, Wipfler B, Wilde F, Misof B. 2014 Head morphology of *Tricholepidion gertschi* indicates monophyletic Zygentoma. *Front. Zool*. **11**, 16. (doi:10.1186/1742-9994-11-16)
73. Blanke A, Machida R, Szucsich NU, Wilde F, Misof B. 2015 Mandibles with two joints evolved much earlier in the history of insects: dicondyly is a synapomorphy of bristletails, silverfish and winged insects. *Syst. Entomol*. **40**, 357–364. (doi:10.1111/syen.12107)
74. Lieven AF. 2000 The transformation from monocondylous to dicondylous mandibles in the Insecta. *Zool. Anz*. **239**, 139–146.
75. Staniczek AH. 2000 The mandible of silverfish (Insecta: Zygentoma) and mayflies (Ephemeroptera): its morphology and phylogenetic significance. *Zool. Anz*. **239**, 147–178.
76. Gröning F, Bright JA, Fagan MJ, O'Higgins P. 2012 Improving the validation of finite element models with quantitative full-field strain comparisons. *J. Biomech*. **45**, 1498–1506. (doi:10.1016/j.jbiomech.2012.02.009)
77. Gröning F, Fagan M, O'Higgins P. 2012 Modeling the human mandible under masticatory loads: which input variables are important? *Anat. Rec. Adv. Integr. Anat. Evol. Biol*. **295**, 853–863. (doi:10.1002/ar.22455)
78. Gröning F, Fagan MJ. 2012 Comment on 'The effects of modelling simplifications on craniofacial finite element models: the alveoli (tooth sockets) and periodontal ligaments' (vol. **44**, issue 10, pages 1831–1838). *J. Biomech*. **45**, 1749–1750. (doi:10.1016/j.jbiomech.2011.10.042)
79. Bright JA, Gröning F. 2011 Strain accommodation in the zygomatic arch of the pig: a validation study using digital speckle pattern interferometry and finite element analysis. *J. Morphol*. **272**, 1388–1398. (doi:10.1002/jmor.10991)
80. Curtis N, Jones MEH, Lappin AK, O'Higgins P, Evans SE, Fagan MJ. 2010 Comparison between *in vivo* and theoretical bite performance: using multi-body modelling to predict muscle and bite forces in a reptile skull. *J. Biomech*. **43**, 2804–2809. (doi:10.1016/j.jbiomech.2010.05.037)
81. Curtis N, Jones MEH, Evans SE, Shi J, O'Higgins P, Fagan MJ. 2010 Predicting muscle activation patterns from motion and anatomy: modelling the skull of Sphenodon (Diapsida: Rhynchocephalia). *J. R. Soc. Interface*. **7**, 153–160. (doi:10.1098/rsif.2009.0139)
82. Charles JP, Cappellari O, Spence AJ, Wells DJ, Hutchinson JR. 2016 Muscle moment arms and sensitivity analysis of a mouse hindlimb musculoskeletal model. *J. Anat*. **229**, 514–535. (doi:10.1111/joa.12461)
83. Kupczik K, Dobson CA, Fagan MJ, Crompton RH, Oxnard CE, O'Higgins P. 2007 Assessing mechanical function of the zygomatic region in macaques: validation and sensitivity testing of finite element models. *J. Anat*. **210**, 41–53. (doi:10.1111/j.1469-7580.2006.00662.x)
84. Sellers WI, Crompton RH. 2004 Using sensitivity analysis to validate the predictions of a biomechanical model of bite forces. *Ann. Anat*. **186**, 89–95. (doi:10.1016/S0940-9602(04)80132-8)
85. Toro-Ibacache V, Fitton LC, Fagan MJ, O'Higgins P. 2016 Validity and sensitivity of a human cranial finite element model: implications for comparative studies of biting performance. *J. Anat*. **228**, 70–84. (doi:10.1111/joa.12384)
86. Tseng ZJ, Mcnitt-Gray JL, Flashner H, Wang X, Enciso R. 2011 Model sensitivity and use of the comparative finite element method in mammalian jaw mechanics: mandible performance in the gray wolf. *PLoS ONE* **6**, e19171. (doi:10.1371/journal.pone.0019171)
87. Watson PJ, Fagan MJ, Dobson CA. 2015 Sensitivity to model geometry in finite element analyses of reconstructed skeletal structures: experience with a juvenile pelvis. *Proc. Inst. Mech. Eng. H* **229**, 9–19. (doi:10.1177/0954411914564476)